Numerical investigation of the discharge characteristics of the pulsed discharge nozzle

B. H. P. Broks, W. J. M. Brok, J. Remy, and J. J. A. M. van der Mullen*
Department of Applied Physics, Eindhoven University of Technology, P.O. Box 513, 5600 MB, Eindhoven, The Netherlands

A. Benidar and L. Biennier
Laboratoire de Physique des Atomes, Lasers, Molécules et Surfaces (PALMS), UMR 6627, Université de Rennes 1, 35042 Rennes Cedex, France

F. Salama
Space Science Division, NASA-Ames Research Center, Moffett Field, California 94035-1000, USA
(Received 22 December 2004; published 23 March 2005)

The characteristics of the plasma generated by a pulsed discharge slit nozzle (PDN) are investigated. The PDN source is designed to produce and cool molecular ions creating an astrophysically relevant environment in the laboratory. A discharge model is applied to this system to provide a qualitative as well as a quantitative picture of the plasma. We find that the plasma's properties and behavior are characteristic of those of a glow discharge. We model the electron density and energy, as well as the argon ion and metastable atom number density. The results reveal a high abundance of metastable argon atoms in the expansion region, which is more than one order of magnitude higher than the abundance of electrons and ions. These findings confirm experimental observations, which concluded that large molecular ions are dominantly formed through Penning ionization of the neutral molecular precursors seeded in the supersonic expansion of argon gas. The simulations presented here will help optimize the yield of formation of molecular ions and radicals in the PDN source; they will also provide key physical insight into the characteristics of interstellar molecules and ions analogs in laboratory experiments.

DOI: 10.1103/PhysRevE.71.036409 PACS number(s): 52.30.Ex, 52.65.Kj, 52.72.+v, 52.80.Hc

I. INTRODUCTION

Carbon containing species such as polycyclic aromatic hydrocarbons (PAHs) are important building blocks of interstellar dust and are detected in meteorite samples and interplanetary dust particles. Observational, laboratory, and theoretical studies have shown that PAHs, in their neutral and ionized forms, are indeed an important and ubiquitous component of the interstellar medium [1]. PAHs might account for two unexplained phenomena, which have been challenging the astrophysical community for almost a century: (a) the unidentified infrared bands observed in the infrared emission spectrum of the interstellar medium (ISM), and (b) the diffuse interstellar bands seen in the visible and the near infrared absorption spectrum of diffuse interstellar clouds [2]. In order to assess the PAH proposal, which was first introduced by Leger and Puget [3] and by Allamandola *et al.* [4], we are constrained to compare astronomical observations with laboratory data, obtained under conditions that come close to those that reign in the ISM. This implies measuring the spectra of neutral and ionized PAHs isolated in the gas phase at low (cryogenic) temperature. Until recently, the best compromise was achieved by trapping PAH molecules in a rare gas solid matrix using matrix isolation spectroscopy. PAHs are large and nonvolatile molecules and the study of cold and ionized PAHs analogs in the gas phase remained an unexplored area until 1999 [5,6].

Supersonic plasma sources have opened new possibilities for the generation of astrochemical species. These sources have been intensively used to produce isolated gas-phase carbon chains, which are cooled down and stabilized in the supersonic expansion, thus facilitating mass or optical detection [7]. Recently, supersonic plasma sources have been used to generate cold PAH cations in the gas phase in number densities high enough to enable the measurement of their optical absorption spectra by cavity ring down spectroscopy [8–10].

Such sources offer a powerful tool to produce and investigate radicals and ions, which are translationally and rovibrationally cold and vibrationally excited [11]. Supersonic expansion sources with long-slit orifices have more particularly proven to be efficient in generating high column densities of molecular ions and radicals, because of the increase in the absorption pathlength [12].

In spite of the potential of supersonic plasma expansions for producing astrochemical species, few studies have been carried out on the characteristics of the plasma generated. The research described in the present paper investigates a pulsed planar expansion generated by a pulsed discharge nozzle (PDN), that has been developed at NASA Ames to generate PAH cations in the gas phase [8].

The PDN source is based on a slit jet mounted in a vacuum chamber (see Fig. 1). The shutter runs at 10 Hz and typically opens for a duration of 1.2 ms, generating intense short gas pulses with flow rates of 8 cm^3 per pulse. Two negatively biased jaws forming the cathode are mounted on each side of the 200 μm wide and 10 cm long slit and are 400 μm apart. They are insulated from the PDN assembly

*Author to whom correspondence should be addressed. Email address: j.j.a.m.v.d.mullen@tue.nl

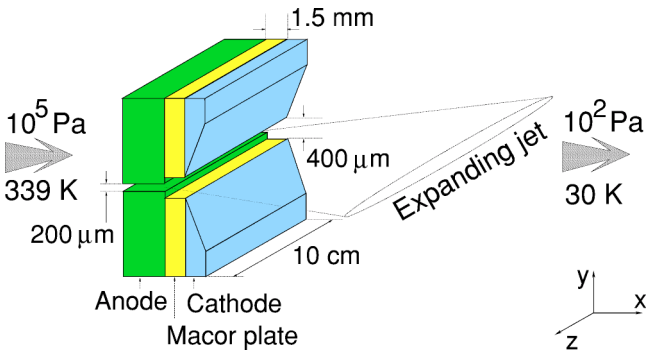

FIG. 1. (Color online) A schematic drawing of the pulsed discharge nozzle. The gas enters at atmospheric pressure on the left side and subsequently expands through the region between anode and cathode, where the discharge is generated.

(anode) by a 1.5 mm thick insulator plate (Macor© plate).

On the left hand side, neutral gas enters with a pressure of approximately 10^5 Pa. The right hand side opening originates in a vacuum chamber, which is pumped to a backing pressure of 20 Pa. Because of this steep pressure gradient, the gas flows through the discharge region and expands supersonically in the vacuum chamber.

A voltage ranging from −400 to −600 V (through 1 kΩ ballast resistors) is applied for 500 μs during the gas pulse, ensuring that electrons flow against the supersonic stream and that the discharge remains confined as well as uniform along the slit. The plasma is thus generated in the expanding gas. The geometry of the source leads to a residence time of a few microseconds for the molecules in the active region of the discharge.

The plasma generated in the PDN source has been experimentally characterized as a glow discharge in the abnormal regime. A detailed qualitative analysis can be found in Refs. [13,14]. Estimates of the electron temperature and electron density in the plasma have been obtained in these studies but do not provide a full and proper comprehensive description of the plasma properties.

In this paper, we will continue the research outlined above. We use a two-dimensional fluid model [15] to gain insight into the physicochemical processes occurring in the PDN source. It will be shown that our model is capable of generating a picture that is qualitatively and quantitatively consistent with the experimental observations from Refs. [13,14].

In Sec. II, we describe the model on which the simulations are based. This includes a brief description of the fluid equations, the data on species and reactions, the representation of the geometry, and how the flow is calculated and taken into account in the discharge model. In Sec. III, we present simulation results on the spatial profile of relevant quantities associated with the plasma. We will also discuss and interpret these results from both a physical and a chemical point of view.

II. MODEL

In this section we will describe the model in its various aspects: the equations that are solved, the data on species and reactions, the numerical approximation of the geometry of the device, and finally the background density field and flow field that we obtained from separate calculations.

A. Model description

In order to describe the PDN numerically, we made use of an existing discharge model and modified it slightly to take the flow of the background gas and the variations in the background gas density into account. This model has previously been used for describing plasma display panel pixels [16] and the ignition of compact fluorescent lamps [15]. It is described fully in Ref. [15] and references therein. Briefly, this is a time-dependent, two-dimensional fluid model, in which several balance equations are solved in conjuncture with the Poisson equation.

The balance equations are solved in the drift diffusion approach for a number of species, such as electronically excited species, ions and electrons, all specified in Sec. II B,

$$\frac{\partial n_p}{\partial t} + \nabla \cdot \mathbf{\Gamma}_p = S_p \tag{1}$$

with

$$\mathbf{\Gamma}_p = \pm \mu_p \mathbf{E} n_p - D_p \nabla n_p + \mathbf{v}_b n_p, \tag{2}$$

where n_p is the density of species p, S_p the source of the species due to reactions, μ_p and D_p the species' mobility and diffusion coefficient respectively, $\mathbf{E}$ the electric field, and $\mathbf{v}_b$ the flow velocity of the background gas. The last term in Eq. (2) has been added, as compared to the model described in Refs. [15,16].

In addition to the balance equations for the various species, a balance equation is included for the electron energy, with a source term representing the energy gained in the electric field and the energy lost in collisions. The inclusion of this equation allows us to specify the various transport and reaction rate coefficients as functions of the mean electron energy. This approach differs from the commonly used local field approximation, in which these quantities are specified as functions of the local electric field strength and the assumption is made that the electron energy is solely determined by local conditions.

The electron transport and reaction rate coefficients were obtained from an external Boltzmann solver [17]. This solver calculates the electron energy distribution function in the pulsed Townsend approximation. From the resulting electron energy distribution functions at different reduced electric field strengths, the various coefficients are calculated as a function of the mean electron energy. These data are used as input to the model via lookup tables. The transport coefficient for the other species and the reaction rate coefficients for heavy particle reactions are taken from the literature and presented to the model as functions of the reduced electric field. These reaction and transport coefficients and the literature from which they originate are listed in Sec. II B.

As mentioned earlier, a distinct feature of the PDN is a gas flow through the device in the direction of the cathode. Since the power dissipated in the discharge is low enough to not cause appreciable gas heating, the flow of the back-

ground gas can be described independently from the discharge. In the discharge model we therefore made use of precalculated velocity and density fields (see Sec. II D for these flow calculations) and used them as fixed input values. The nonuniform density field influences itself by its influence on the reduced electric field and thus on the source term in Eq. (1) and the various transport coefficients in the drift diffusion Eq. (2). The velocity field enters as an extra term in Eq. (2). Especially for the neutral species, the flow term forms an important contribution to the fluxes of these species.

As mentioned earlier, refer to Ref. [15] for the full set of equations, including boundary conditions. These equations are discretized on a rectangular uniform grid and solved via a control volume method.

B. Species

In this first paper we assume that the presence of PAHs, which are highly diluted in the argon carrier gas (less than 1%), does not affect the discharge behavior appreciably.

The set of species and reactions that we incorporated in the model is equivalent to the one used in Ref. [15]. Briefly, the set of species consists of the electrons e, three effective excited states of argon, and the argon ion Ar^+. The first effective excited state, denoted Ar^*, represent the four levels in the 4*s* manifold of argon. This species is assumed to be metastable because the electron impact cross section for creating a metastable 4*s* level is significantly larger than the cross section for creating a resonant 4*s* level. The second excited state, denoted Ar^{**}, represents the 4*p* manifold and higher levels. In order to take into account collisional quenching of the two metastable states to the two resonant states in the 4*s* manifold, a third excited species Ar_r^* is specified, which is destroyed by deexcitation to the ground level. The transport coefficients for these species are obtained from Refs. [17–20]. The value of the secondary emission coefficient for Ar^+ on the electrode materials is strongly dependent on the quality of the surface, which is unknown. In this paper we use an estimated value of 0.01 electrons per incident ion.

The various reactions that are included in the model are listed in Table I, including the original references to the literature from which the cross sections or rate coefficients were obtained. Note that the reaction rate coefficient for reactions in which electrons are involved were calculated using the above-mentioned Boltzmann solver.

We do not take electron-electron collisions into account. Since the ionization degree is low and the electron density fairly high, inelastic collisions with the background gas are more common than electron-electron collisions. This is true in particular for the sheaths, where most of the reaction kinetics takes place.

C. Geometry

As schematically shown in Fig. 1 and described in more detail in the introductory section, the pulsed discharge nozzle is composed of two electrode plates, separated by an insulator plate. A large aspect-ratio slit in this structure forms the discharge region, of which a cross section is shown in Fig. 2.

TABLE I. The reaction rate coefficients used by the model.

No.	Reaction	Reference
0	$Ar+e \rightarrow Ar+e$	[21]
1	$Ar+e \rightarrow Ar^*+e$	[22]
2	$Ar+e \rightarrow Ar^{**}+e$	[22]
3	$Ar+e \rightarrow Ar^+ +2e$	[21]
4	$Ar^*+e \rightarrow Ar+e$	[22][a]
5	$Ar^*+e \rightarrow Ar^{**}+e$	[23]
6	$Ar^*+e \rightarrow Ar^+ +2e$	[24]
7	$Ar^{**}+e \rightarrow Ar+e$	[22][a]
8	$Ar^{**}+e \rightarrow Ar^*+e$	[23][a]
9	$Ar^{**}+e \rightarrow Ar^*+2e$	[25]
10	$Ar^*+Ar^* \rightarrow Ar^+ +Ar+e$	[26]
11	$Ar^*+Ar^{**} \rightarrow Ar^+ +Ar+e$	[26]
12	$Ar^{**}+Ar^{**} \rightarrow Ar^+ +Ar+e$	[26]
13	$Ar^*+e \rightarrow Ar_r^*+e$	[27,28]
14	$Ar_r^* \rightarrow Ar+h\nu$	[15]
15	$Ar^{**} \rightarrow Ar^*+h\nu$	[15]

[a]From the forward reaction using microscopic reversibility.

Experimental measurements show that the discharge has the positive current-voltage characteristic that is typically associated with an abnormal glow. This means that the discharge covers the whole electrode along the length of the slit, as opposed to the partial coverage that one would find in the normal glow regime. Given the nature of the plasma, and given the large aspect ratio of the slit, the device can be represented by a two-dimensional model. The Cartesian coordinates x and y thus describe the direction from anode to cathode and the direction perpendicular to this, respectively (see Fig. 2). The omitted z direction points along the length of the slit.

Note that the device is mirror symmetric with respect to the center plane of the slit. We therefore only need to describe one side of it. Also, the current is expected to run

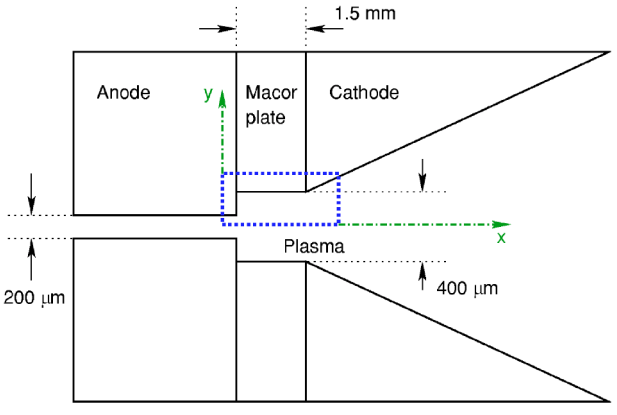

FIG. 2. (Color online) A schematic drawing of the geometry of the pulsed discharge nozzle. The size of the central plasma channel is exaggerated for clarity. The dashed square is the part of the device that is simulated. The gas flows from a high-pressure source on the left to a vacuum chamber on the right.

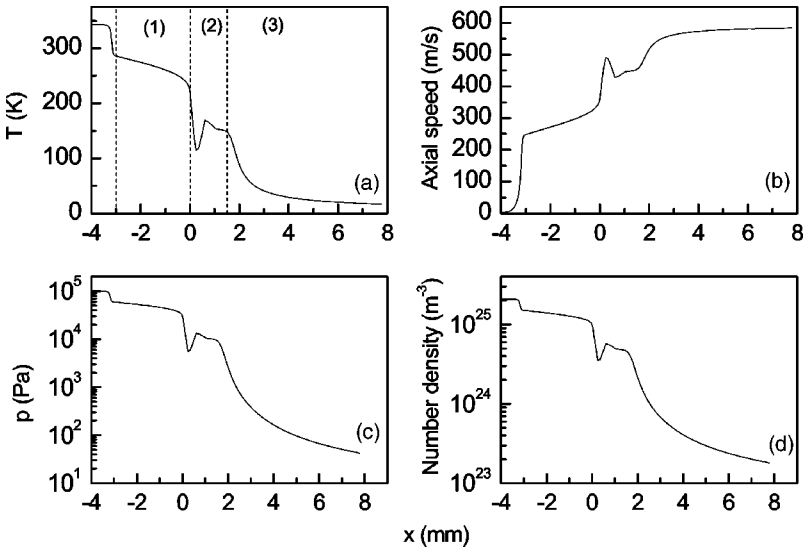

FIG. 3. Key thermodynamic parameter profiles along the flow axis center line, obtained for an Ar backing pressure of 10^5 Pa and a reservoir temperature of 339 K.

between the sections of the anode and the cathode that are the closest to each other. As a result, the calculation domain of the discharge will be confined to a small region along the *x* axis in the channel. Our simulation will thus focus on the region highlighted in the figure. The validity of the latter assumption will be discussed in a later section.

Finally, since the time scale needed by the discharge to reach steady state was found to be small compared to the typical discharge pulse length of 500 μs, we consider a dc operated discharge only. The ballast resistor in series with the discharge was set to 10 kΩ/cm, corresponding to 1 kΩ for the slit length of 10 cm.

D. Bulk flow

The PDN flow is modeled by a separate computer program MB-CNS that can calculate transient compressible flows in two-dimensional geometries. It is based on a finite volume formulation of the Navier-Stokes equations [29,30]. For the reasons stated above, the problem is considered in two dimensions.

The program takes the following quantities as input: the geometry of the source, the molecular mass, viscosity, thermal conductivity, and heat capacity of the gas, and finally the initial conditions, consisting of the reservoir temperature and pressure. From these parameters, the program calculates a grid and subsequently the temperature, pressure, mass density, velocity, and Mach number of the flow profile.

The results of the two-dimensional flow simulation are described in detail in Ref. [31]. Only the main relevant features are briefly summarized below.

The physical conditions are calculated for long hydrodynamic times, close to the stationary regime (>1 ms). The profiles of the key thermodynamic parameters along the flow axis center line are shown in Fig. 3.

Three zones can be distinguished in the flow pattern: (1) the gas injection channel, (2) the discharge region, and (3) the postdischarge region. The flow velocity steadily increases in the injection channel but remains subsonic. The expansion becomes supersonic (Mach number $M>1$) at the beginning of the second zone. The sudden growth of the Mach number in the first $\sim$200 μm is followed by a drop in the next $\sim$200 μm, caused by the compression of the expansion by the walls of the interelectrode region. Then the Mach number gradually rises in the remaining 1.1 mm to achieve Mach 2 at the tip of the cathode. Finally, the postdischarge zone is characterized by the typical behavior of planar expansions with a temperature that is inversely proportional to the distance from the exit.

III. RESULTS AND DISCUSSION

A. Introduction

Using the model presented in Sec. II, we simulated the pulsed discharge nozzle for a source voltage of -500 V. By using the time-dependent equations described in Sec. II on a suitable starting condition, a steady-state solution (differing less than 1% from the solution after a much longer time of 50 μs) is obtained in less than 15 μs. This is much shorter than the typical discharge time of 0.5 ms [8], meaning that stable conditions are present during most of the discharge. The discussion is restricted to this stable situation.

The plasma is analyzed, mainly using contour maps of the five most important physical quantitities: The electron density n_e, in Fig. 4; the argon ion density n_{Ar^+}, in Fig. 6; the voltage V, in Fig. 7; the average electron energy ε, in Fig. 8; the argon metastable density n_{Ar^*}, in Fig. 9. Each of these figures will be discussed. Finally, we will present some results of operation at different source voltages.

B. The electron density

The electron number density is shown in Figs. 4 and 5. It is, as expected, very small ($<1\times10^{17}$ m^{-3}) both in the interelectrode sheath, which lies under the insulating plate, and in the cathode fall near the surface of the cathode.

In the case of the interelectrode sheath, this is to be expected, as the ambipolar flux of the plasma to the wall and the recombination at the wall will cause an electron density which is lower than in the plasma bulk. The interelectrode

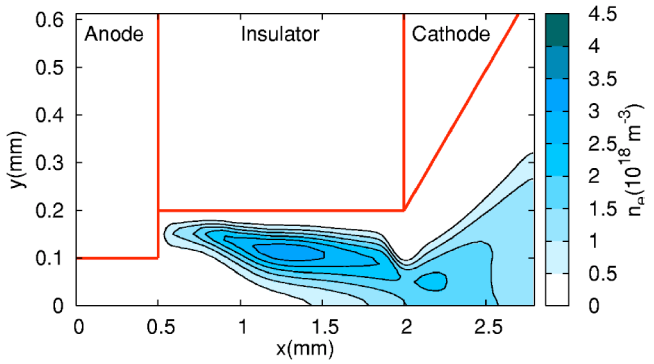

FIG. 4. (Color online) The steady-state electron density of the pulsed discharge nozzle for a source voltage of −500 V. The color bar and isolines range from 0 to 4.5×10^{18} m^{-3} in steps of 5×10^{17} m^{-3}. The bold lines indicate the different parts of the device.

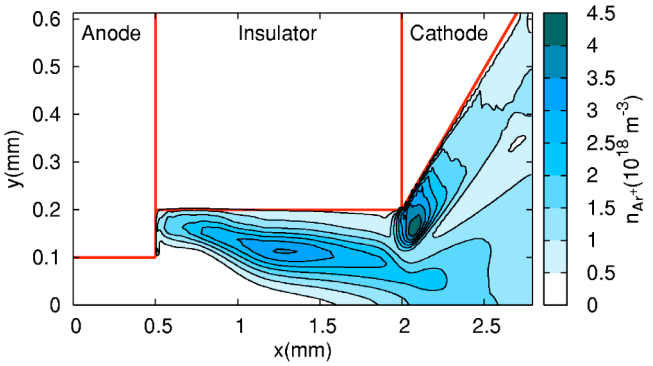

FIG. 6. (Color online) The steady-state Ar^+ density of the pulsed discharge nozzle for a source voltage of −500 V. The color bar and isolines range from 0 to 4.5×10^{18} m^{-3} in steps of 5×10^{17} m^{-3}. The bold lines indicate the different parts of the device.

sheath thickness ranges from about 25 μm near the anode to 100 μm near the cathode. This should be equal to several times the Debye length λ_D, which is given by Ref. [32]:

$$\lambda_D = \sqrt{\frac{\varepsilon_0 k_B T_e}{n_e e^2}}. \tag{3}$$

Substituting a value for n_e of 3×10^{18} m^{-3} (from Fig. 5) and a value for T_e of 3 eV (from Fig. 8), which are both typical for the central area between the insulating plates, in Eq. (3), we obtain a value of 8 μm for λ_D. The interelectrode sheath is several times λ_D near the cathode, as expected, but near the anode, it is thinner because the plasma is pushed to the wall by the internal expansion.

In the cathode fall region, the electron density is also low. This is caused by the presence of a positive space charge, characteristic for this region.

The central electron density of the device reaches values of up to 3.4×10^{18} m^{-3}. Along the cathode, the discharge becomes less intense further away from the tip. This is caused by the variation in the gas density, which is the highest near the electrode tip and drops when moving further away from it. This lowering of the background gas density means that collisions between electrons and atoms of the background gas become less frequent; hence the ionization degree decreases. This furthermore implies that only a small part of the electrode is in fact responsible for the bulk of the plasma production. This justifies, *a posteriori*, not simulating the full cathode, but only the areas that are the closest to the outflow opening.

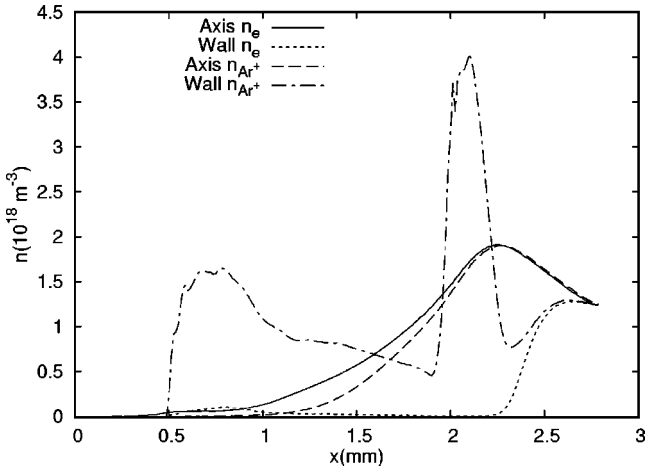

FIG. 5. The steady-state density of Ar^+ and electrons of the pulsed discharge nozzle for a source voltage of −500 V, at the symmetry plane at $y=0$ mm and near the wall at $y=0.1875$ mm.

C. The Ar^+ density

The Ar^+ density in the discharge is depicted in Figs. 5 and 6. There is a zone with a low ($<5\times10^{17}$ m^{-3}) Ar^+ density in the center of the channel, near the anode. There is a distinctive ridge near the cathode surface, where the Ar^+ density is high, reaching a maximum near the tip and dropping off along the cathode surface.

Between the insulating plates, the Ar^+ density is nearly equal to the electron density of about 3×10^{18} m^{-3}, indicating a quasineutral plasma.

Near the cathode, however, the Ar^+ density is far higher than the electron density, reaching values of up to 4.5×10^{18} m^{-3}. This creates a band of positive space charge close to the cathode, with a maximum space charge of 0.72 C m^{-3}. This band causes the cathode fall region of the plasma. It is noted that the difference between the electron density and the Ar^+ density is the highest near the tip of the cathode. This also means that the net space charge is the highest there. This is consistent with the cathode being more efficient in the region displaying the highest background gas density, as explained in Sec. III B.

Furthermore, there is an area of low Ar^+ density near the symmetry plane of the plasma on the anode side. This is caused by the interelectrode expansion, which pushes ions toward the insulating plate. Because of the high densities of charged particles and modest fields between the plates, significant deviations from quasineutrality cannot occur in this region. Hence, the electron density also becomes low in this

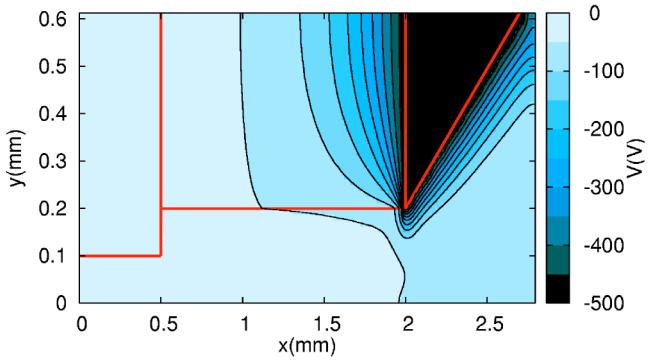

FIG. 7. (Color online) The steady-state voltage of the pulsed nozzle discharge for a source voltage of −500 V. The color bar and isolines range from −500 to 0 V in steps of 50 V. The bold lines indicate the different parts of the device.

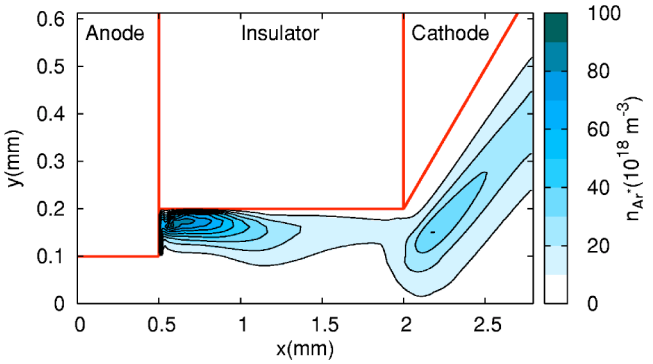

FIG. 9. (Color online) The steady-state Ar^* density of the pulsed nozzle discharge for a source voltage of −500 V. The color bar and isolines range from 0 to 100×10^{18} m^{-3} in steps of 10×10^{18} m^{-3}. The bold lines indicate the different parts of the device.

area (Fig. 4). As can be seen in Fig. 5, the electron density at the symmetry plane is higher than the ion density between the isolating plates, indicating that the lighter and faster electrons can diffuse somewhat further upstream than the heavier ions before the resulting space charge fields contain them.

D. The voltage

The voltage V in the discharge is depicted in Fig. 7. The cathode, which is at −476 V, is clearly visible. The difference between the source voltage and the cathode voltage is due to the voltage drop over the electrode ballast resistor.

A sharp drop in voltage over the cathode fall is also visible. Because of this, the voltage in the rest of the discharge is rather uniform, and consequently the electric field is small. This is commonly the case in glow discharges [33].

E. The electron energy ε

Figure 8 depicts the average electron energy ε in the discharge on a logarithmic scale. In the cathode fall, ε is in the order of 60 eV, far higher than the ionization energy of argon. Hence, a strong ionization of argon is expected there.

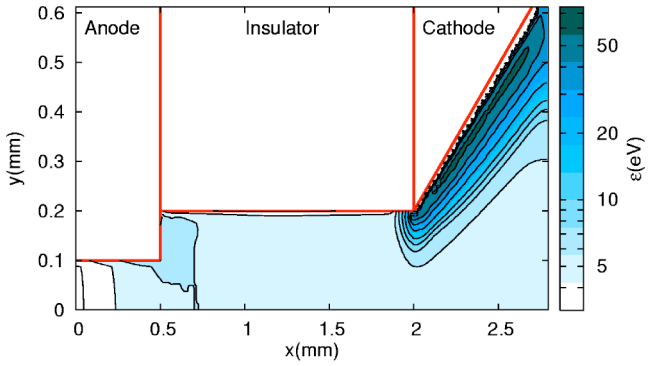

FIG. 8. (Color online) The steady-state average electron energy ε of the pulsed discharge nozzle for a source voltage of −500 V. Notice that the color map is logarithmic, and ranges from 3.16 to 74.8 eV. The bold lines indicate the different parts of the device.

This is consistent with the results in Figs. 4 and 6. In the interelectrode region, ε is about 4 eV. Near the anode, ε is significantly higher, 6 eV. This is due to the compression of the plasma by the internal expansion, which increases the local dissipation density. In the expansion zone, however, the electric field is small, which results in little heating of the electrons, and a drop in their temperature down to 5 eV is seen in the simulation domain. This indicates that electron kinetics are mostly important near the cathode.

The dissociation energy of PAHs is significantly lower than the ionization energy. This means that processes involving bulk electrons, which have mean electron energies of about 5 eV, are far more likely to dissociate rather than ionize the PAH, as the density of electrons with an energy above the dissociation threshold is far higher than the density of electrons with an energy above the ionization threshold. In this plasma, both average electron energy and density are fairly low, especially in the downstream area, so electron excitation kinetics are of minor importance.

The high value of ε in the cathode fall means that the bulk of the electrons have sufficient energy to ionize argon on impact. The ionization rate thus mainly depends on the background gas density.

F. The Ar^* density

The Ar^* density in the discharge is depicted in Fig. 9. It can be seen that metastable argon can reach high densities, with a maximum density that is 20 and 30 times higher than the maximum Ar^+ and e densities, respectively. There are two production centers of Ar^* in the simulation domain: one near the anode and one near the cathode tip. The chief mechanism of transport of Ar^* is bulk flow, as the flow is fast in this plasma compared to the diffusion, and neutral Ar^* is not subject to drift induced by electric fields. This is clearly visible in Fig. 9, as expanding plumes of Ar^* follow the bulk flow coming from the production zones.

High number densities of Ar^* are generated in the plasma due to the significant fraction of electrons with an energy higher than 11.5 eV and the large Ar excitation cross section. The results show that Ar^* is more abundant in the plasma by more than one order of magnitude than electrons with an

energy above the PAH ionization potential. Therefore, the production of PAH cations by Penning ionization should dominate over electron impact ionization assuming cross sections of the same magnitude based on the scarce data available [4.2×10^{-20} m^2 for Penning ionization of C_{60} with Ar^* ($4p\,^3D_3$) [34] and $<10^{-20}$ m^2 for electron impact ionization (12 eV) of C_{60} [35]]. These results are confirmed by previous experimental observations [8].

G. Other source voltages

Based on the five plasma parameters discussed earlier, n_e, n_{Ar^+}, V, ε, and n_{Ar^*}, and further calculations not detailed here, such as numerical experiments in which the background gas density and flow velocity are varied, we will now discuss the mechanisms that are responsible for the operation of the pulsed discharge nozzle as a chemical source of cold PAH ions.

Because of the unusual geometry of the source, the variations in background gas density, and the presence of a significant bulk flow, it is not possible to solely look at classical gas discharge theory to adequately explain the operation of the pulsed discharge nozzle.

In a normal glow, the current can vary with only minimal variations in voltage. This is because the cathode is only partially covered with an electron-emitting cathode fall. Increasing or decreasing the area covered changes the amount of electrons emitted and consequently the current but does not change the voltage, provided the cathode surface and gas composition near the cathode are homogeneous.

In this device, the variations in the background gas density near the cathode mean that parts of the cathode fall will produce electrons more easily than others. This device will thus not exhibit the current-voltage behavior typical of a normal glow, as increasing the active area of the cathode would require using parts of the cathode which are less prone to electron emission due to the lower background density, which would require the voltage to rise when the current rises.

In addition to the results presented above, we have simulated the pulsed discharge nozzle for a variety of input voltages. A graph of the current density in the device is given in Fig. 10. Below −380 V, no stable solution is found. The current-voltage relation is positive, which is consistent with the above explanation.

Experimental data in Ref. [13] also show a positive current-voltage characteristic. Generally, the quantitative match between the measured and simulated voltage is excellent, the measured currents being 30% lower than the simulated data at most, while the threshold voltage matches within 2%. A better match cannot be expected given that many input parameters, such as reaction cross sections and the secondary emission coefficient, are not known to such a precision.

The discrepancy between the simulated and experimental current-voltage characteristics gives an indication of the error of the computed values of n_e and n_{Ar^+}, which are expected to be of the same magnitude, as the conductivity is dependent on these parameters. This puts the expected error in n_e and n_{Ar^+} at around 50%. The error in n_{Ar^*} is expected to be of a similar magnitude.

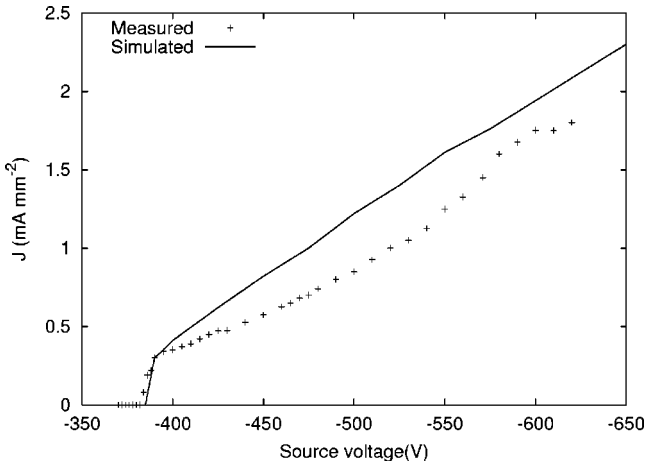

FIG. 10. The simulated (solid line) and measured (crosses) current of the pulsed discharge nozzle as a function of source voltage.

IV. CONCLUSIONS

We have developed a model of the pulsed discharge nozzle and used it to obtain values for key plasma parameters and to gain insight into the physical processes that determine its behavior.

The plasma in the pulsed discharge nozzle is clearly a glow discharge, with a current-voltage characteristic typical of the abnormal regime. The plasma has a cathode fall near the cathode, a plasma sheath that separates it from the insulating wall, and a quasineutral bulk. For the typical operating voltages, the electron density is in the order of 3×10^{18} m^{-3}, which is at the high end of the value range that is typical for glow discharges.

The shape of the cathode and the variations in the density of the background gas cause the cathode to be most active near its tip. This also means that the current-voltage characteristics may be quite different from those of a standard parallel-plate glow discharge.

The argon metastables that are formed are not affected by the electric field, and therefore can be transported downstream easily. This reduces the chance of quenching and stepwise ionization, boosting the ratio of metastables to ions and strongly enhancing the behavior of the PDN as a source of cold metastable noble gas atoms. A numerical model in which flow was excluded has confirmed this behavior.

The low electron temperature in the expansion zone causes PAH ionization by electron impact to be of less importance. The flux of cold, metastable argon, with a well-defined excitation energy, makes it possible to ionize PAHs with limited fragmentation. By choosing a suitable noble carrier gas, the reaction energy can be adjusted as necessary. These traits make this PDN source particularly suitable for generation of astrochemically relevant species.

A comparison between the simulated and measured

current-voltage characteristics shows an excellent match over the complete range of simulated voltages. This indicates n_e is computed accurately, and suggests the densities of the other plasma species are accurately computed as well.

Using this model, a controlled parameter study can now be performed by varying the background gas mixture and/or the geometry of the source to optimize the yield of metastable carrier gas atoms and, hence, the yield of interstellar analogs in the laboratory.

ACKNOWLEDGMENTS

This project is supported under the NASA Science Mission Directorate APRA program and NASA Ames DDF project. B.H.P.B., W.J.M.B., and J.R., respectively, acknowledge support from the Stichting voor Fundamenteel Onderzoek der Materie (FOM), from Philips Research, and from the Center for Plasma Physics and Radiation Technology (CPS).

[1] F. Salama, in *Solid Interstellar Matter: The ISO Revolution*, edited by L. d'Hendecourt, C. Joblin, and A. Jones, Les Houches Workshop, 1998 (EDP Sciences/Springer-Verlag, Les Ullis, 1999), p. 65.
[2] A. Evans, *The Dusty Universe* (Ellis Horwood, London, 1994).
[3] A. Leger and J. L. Puget, Astron. Astrophys. **137**, L5 (1984).
[4] L. J. Allamandola, A. G. G. M. Tielens, and J. R. Barker, Astrophys. J., Lett. Ed. **290**, L25 (1985).
[5] D. Romanini, L. Biennier, F. Salama, A. Kachanov, L. J. Allamandola, and F. Stoeckel, Chem. Phys. Lett. **303**, 165 (1999).
[6] P. Bréchignac and T. Pino, Astron. Astrophys. **343**, L49 (1999).
[7] E. Witkowicz, H. Linnartz, C. A. de Lange, W. Ubachs, A. Sfounis, M. Massaouti, and M. Velegrakis, Int. J. Mass. Spectrom. **232**, 25 (2004).
[8] L. Biennier, F. Salama, L. J. Allamandola, and J. J. Scherer, J. Chem. Phys. **118**, 7863 (2003).
[9] O. Sukhorukov, A. Staicu, E. Diegel, G. Rouillé, Th. Henning, and F. Huisken, Chem. Phys. Lett. **386**, 259, (2004).
[10] L. Biennier, F. Salama, M. Gupta, and A. O'Keefe, Chem. Phys. Lett. **387**, 287 (2004).
[11] S. Davis, D. T. Anderson, G. Duxbury, and D. J. Nesbitt, J. Chem. Phys. **107**, 5661 (1997).
[12] D. T. Anderson, S. Davis, T.-S. Zwier, and D. J. Nesbitt, Chem. Phys. Lett. **258**, 207 (1996).
[13] J. Remy, L. Biennier, and F. Salama, Plasma Sources Sci. Technol. **12**, 295 (2003).
[14] J. Remy, L. Biennier, and F. Salama, Plasma Sources Sci. Technol. **12**, 619, (2003).
[15] W. J. M. Brok, J. van Dijk, M. D. Bowden, J. J. A. M. van der Mullen, and G. M. W. Kroesen, J. Phys. D **36**, 1967 (2003).
[16] G. J. M. Hagelaar, M. H. Klein, R. J. M. M. Snijkers, and G. M. W. Kroesen, J. Appl. Phys. **89**, 2033 (2001).
[17] Computer code BOLSIG, CPA Toulouse & Kinema Software, 1996, freeware, available at http://www.siglo-kinema.com/bolsig.htm
[18] E. W. McDaniel, *Collision Phenomena in Ionized Gases* (John Wiley & Sons, New York, 1964).
[19] *Handbood of Physical Quantities*, edited by I. S. Grigoriev and E. Z. Meilikhov (CRC Press, Boca Raton, FL, 1997).
[20] H. W. Ellis, R. Y. Pai, E. W. McDaniel, E. A. Mason, and L. A. Viehland, At. Data Nucl. Data Tables **17**, 177 (1976).
[21] A. V. Phelps and Z. Lj. Petrović, Plasma Sources Sci. Technol. **8**, R21 (1999).
[22] K. Tachibana, Phys. Rev. A **34**, 1007 (1986).
[23] P. Zapesochnyi and L. L. Shimon, Opt. Spectrosc. **11**, 155 (1966).
[24] R. H. McFarland and J. D. Kinney, Phys. Rev. **137**, A1058 (1965).
[25] L. Vriens, Phys. Lett. **8**, 260 (1964).
[26] A. N. Klucharev and V. Vujnovic, Phys. Rep. **185**, 55 (1990).
[27] N. L. Bassett and D. J. Economou, J. Appl. Phys. **75**, 1931 (1994).
[28] S. Ashida, C. Lee, and M. A. Lieberman, J. Vac. Sci. Technol. A **13**, 2498 (1995).
[29] P. A. Jacobs, NASA Langley Research Center, ICASE Interim Report No. 18, 1991 (unpublished).
[30] P. A. Jacobs, Computer code MB-CNS, Department of Mechanical Engineering, The University of Queensland, 1996 (unpublished).
[31] L. Biennier, A. Benidar, and F. Salama (unpublished).
[32] M. Mitchner and Charles H. Kruger, Jr., *Partially Ionized Gases* (John Wiley & Sons, New York, 1973).
[33] Yu. P. Raizer, *Gas Discharge Physics* (Springer, Berlin, 1991).
[34] J. M. Weber, K. Hansen, M. W. Ruf, and H. Hotop, Chem. Phys. **239**, 271 (1998).
[35] S. Matt, B. Dünser, M. Lezius, H. Deutsch, K. Becker, A. Stamatoic, P. Scheier, and T. D. Märk, J. Chem. Phys. **105**, 1880 (1996).